

PAPER • OPEN ACCESS

## Atmospheric pressure plasma-assisted femtosecond laser engraving of aluminium

To cite this article: Christoph Gerhard *et al* 2018 *J. Phys. D: Appl. Phys.* **51** 175201

View the [article online](#) for updates and enhancements.

### Related content

- [Femtosecond laser ablation behavior of gold, crystalline silicon, and fused silica: a comparative study](#)  
M E Shaheen, J E Gagnon and B J Fryer
- [Experimental study on 785 nm femtosecond laser ablation of sapphire in air](#)  
M E Shaheen, J E Gagnon and B J Fryer
- [Solar cell thin film processing](#)  
J Hermann, M Benfarah, S Bruneau et al.





**IOP | ebooks™**

Bringing you innovative digital publishing with leading voices to create your essential collection of books in STEM research.

Start exploring the collection - download the first chapter of every title for free.

# Atmospheric pressure plasma-assisted femtosecond laser engraving of aluminium

Christoph Gerhard<sup>1,6</sup>, Thomas Gimpel<sup>2</sup>, Daniel Tasche<sup>3</sup>, Jennifer Koch née Hoffmeister<sup>3</sup>, Stephan Brückner<sup>3,4</sup>, Günter Flachenecker<sup>5</sup>, Stephan Wieneke<sup>3</sup>, Wolfgang Schade<sup>5</sup> and Wolfgang Viöl<sup>3,4</sup>

<sup>1</sup> Faculty of Engineering and Natural Sciences, Technical University of Applied Sciences Wildau, Hochschulring 1, 15745 Wildau, Germany

<sup>2</sup> Clausthal University of Technology, Research Center Energy Storage Technologies, Am Stollen 19A, 38640 Goslar, Germany

<sup>3</sup> Faculty of Natural Sciences and Technology, University of Applied Sciences and Arts, Von-Ossietzky-Straße 99, 37085 Göttingen, Germany

<sup>4</sup> Fraunhofer Institute for Surface Engineering and Thin Films, Application Center for Plasma and Photonics, Von-Ossietzky-Straße 100, 37085 Göttingen, Germany

<sup>5</sup> Fraunhofer Heinrich Hertz Institute, Energie Campus, Am Stollen 19H, 38640 Goslar, Germany

E-mail: [christoph.gerhard@th.wildau.de](mailto:christoph.gerhard@th.wildau.de) and [wolfgang.vioel@hawk-hhg.de](mailto:wolfgang.vioel@hawk-hhg.de)

Received 15 January 2018, revised 9 March 2018

Accepted for publication 15 March 2018

Published 9 April 2018



## Abstract

In this contribution, we report on the impact of direct dielectric barrier discharge argon plasma at atmospheric pressure on femtosecond laser engraving of aluminium. It is shown that the assisting plasma strongly affects the surface geometry and formation of spikes of both laser-engraved single lines and patterns of adjacent lines with an appropriate overlap. Further, it was observed that the overall ablation depth is significantly increased in case of large-scale patterning whereas no notable differences in ablation depth are found for single lines. Several possible mechanisms and underlying effects of this behaviour are suggested. The increase in ablation depth is supposed to be due to a plasma-induced removal of debris particles from the cutting point via charging and oxidation as supported by EDX analysis of the re-solidified debris. Furthermore, the impact of a higher degree of surface wrinkling as well as direct interactions of plasma species with the aluminium surface on the ablation process are discussed.

Keywords: atmospheric pressure plasma, laser-plasma-processing, femtosecond laser machining, dielectric barrier discharge, micro structuring, aluminium

(Some figures may appear in colour only in the online journal)

## 1. Introduction

In the last few years the introduction of atmospheric pressure plasmas (APP) to laser material processing tasks has become a growing field of research. The goal of such APP-laser coupling is to benefit from the combination of plasma- and

laser-induced phenomena in order to increase the efficiency of laser processes and to enable the development of novel laser-based methods. For this purpose, APPs provide a number of technically usable features. Depending on the particular discharge type and electrical operation parameters, either plasma-chemical or plasma-physical mechanisms can be generated and used; a combination of both is also possible. Here, the composition of the process gas mixture as well as the working distance have a significant influence on the nature of the plasma and its mode of operation, respectively, resulting in a high versatility of plasmas. This versatility opens a wide

<sup>6</sup> Author to whom any correspondence should be addressed.



Original content from this work may be used under the terms of the [Creative Commons Attribution 3.0 licence](https://creativecommons.org/licenses/by/3.0/). Any further distribution of this work must maintain attribution to the author(s) and the title of the work, journal citation and DOI.

range of applications. In terms of APP-laser coupling, two different approaches, sequential and simultaneous laser-plasma-processing can be chosen.

The first approach is based on plasma pre-treatment of the work piece surface before laser processing in order to achieve a modification of its optical properties and an increase in absorption in particular [1–4]. For simultaneous laser-plasma-processing, direct interactions between laser irradiation, plasma, and the work piece surface are employed in the course of the ablation process. For example, APP provide a considerable amount of free electrons which are able to excite surface-adherent bonds (e.g. hydrocarbons) via electron impacts on the surface. Such electron-induced excitations lead to a reduction in laser energy required for breaking these bonds. This effect was already used for the removal of lacquer coats [5], parylene C (i.e. a hydrocarbon-based polyxylylene polymer) coatings [6] and for cleaning of artworks [7] where plasma jets were introduced to the actual laser process. Another technically usable effect is a plasma-induced reduction of reaction products during laser ablation when applying nitrogenous and hydrogenous process gases. Based on this mechanism, the formation of burrs and re-solidified debris can be mitigated in the course of APP-assisted laser engraving of stainless steel [8].

In addition, direct dielectric barrier discharge (D-DBD) configurations, where the work piece represents an essential part of the discharge geometry, have turned out to be suitable for increasing the efficiency of different laser processes. For instance, this approach allows an increase in crystallisation efficiency of amorphous silicon to poly-crystalline silicon by a factor of up to 1.95 when introducing argon D-DBD plasma to excimer laser annealing (ELA) [9]. This configuration was also shown to be suitable for increasing the ablation rate during laser drilling of different media such as optical glasses [10], ceramics [11], and aluminium [12].

Until now, experiments on the combination of APP and laser irradiation were merely performed using nanosecond laser sources. However, materials processing with ultrafast lasers provide unique advantages in comparison to conventional nanosecond laser processing techniques [13, 14]. Thermal diffusion towards the surrounding area of the laser-irradiated zone occurs on a time scale which is longer than the interaction time with a single femtosecond laser pulse. If the repetition rate of the femtosecond laser is not exceeding a certain limit, thermal heat is not accumulated and disturbing, well-known effects such as melting or re-solidification and debris formation are suppressed. This enables a precise energy deposition into the material in a locally-selective manner. Ideally, the modified area can be limited to the central area of the focal spot if the laser intensity is adjusted to match the single pulse threshold intensity for ablation. In vacuum, thermal evaporation at the ablation threshold and below that threshold is completely negligible for femtosecond laser pulses. Interestingly, experiments revealed that ablation thresholds for several metals in air are less than half of those measured in vacuum. Gamely *et al* [15] consider collisions between the gas atoms and the surface to be responsible for this, affecting a reduced lifetime of non-equilibrium surface states and allowing thermal evaporation to proceed before the surface cools down.

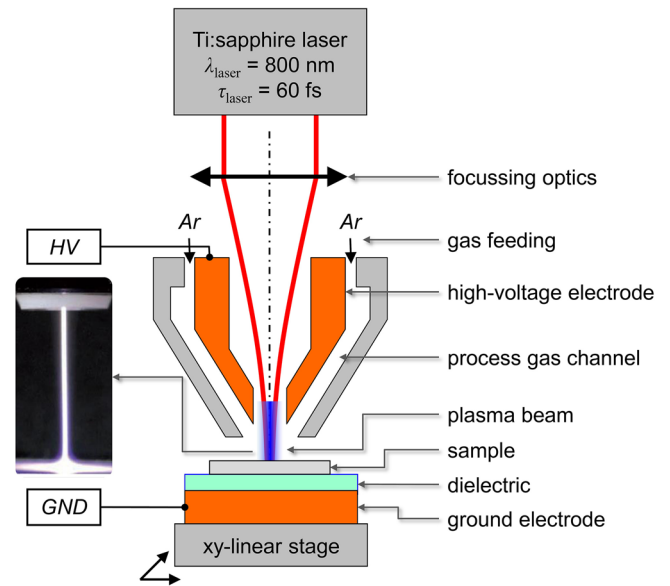


**Figure 1.** Experimental setup for simultaneous APP-assisted femtosecond laser engraving of aluminium samples.

So far, material processing by laser pulses in the femtosecond range has been used with the purpose of structuring [16, 17], hyperdoping [18, 19], micromachining [20], and surface functionalization such as hydrophobicity [21, 22] and customised optical properties [17, 23, 24]. Based on the promising results obtained by combining plasmas and laser irradiation as presented above and the advantageous properties of femtosecond laser irradiation, the influence of D-DBD argon plasmas on femtosecond laser ablation of aluminium was investigated as presented in this work. To our best knowledge, the present contribution is the first work on the simultaneous combination of direct dielectric barrier discharge atmospheric pressure plasma and femtosecond laser irradiation for material processing.

## 2. Experimental

For simultaneous APP-assisted femtosecond laser ablation of aluminium, a conical rotation-symmetric plasma nozzle as described in more detail in [25] was used as plasma source. This plasma source consists of a high-voltage (HV) hollow-core copper electrode which features a central through-hole with a diameter of 3 mm. This special configuration allows the realisation of a common-path alignment of both the plasma and a focused laser beam as shown in figure 1.

The HV-electrode is embedded in a plastic housing made of polyoxymethylene (POM) where the gas channel for feeding the plasma process gas is found between the HV-electrode and the housing. In the present work, argon (Ar 5.0, Linde Gas AG) was used as process gas. Due to the process gas flow, a confined plasma beam with a diameter of approx. 200  $\mu\text{m}$  and a maximum length of 20 mm is formed. As ground (GND) electrode, a dielectrically separated external counter electrode was used. The aluminium samples were placed within the resulting discharge gap where the working distance (plasma outlet nozzle—work piece surface) was approx. 10 mm. The

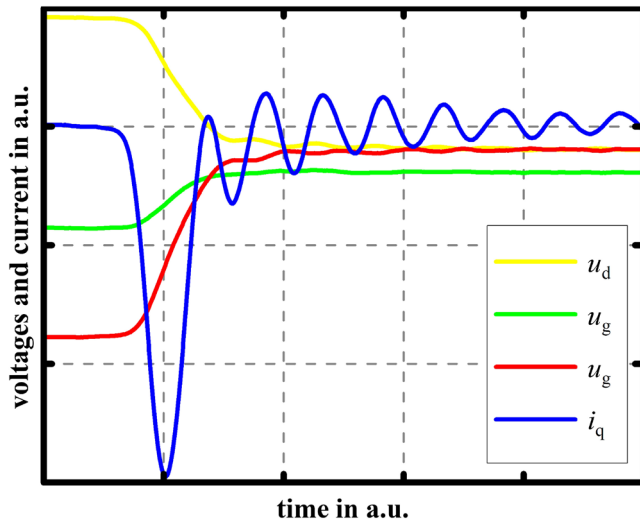


**Figure 2.** Quantitative representation of the current and voltage waveforms of the plasma with  $i_q$  being the current,  $u_d$  being the voltage across the dielectric,  $u_t$  being the total voltage and  $u_g$  being the voltage across the discharge gap.

resulting plasma is thus a D-DBD which primarily affects the surface of the samples. The plasma source was driven by a pulsed power supply at a voltage of  $U_{\text{HV-pulse}} = 11 \text{ kV}$  and a nominal HV-pulse repetition rate of  $f_{\text{HV-pulse}} = 7 \text{ kHz}$ . The pulse duration of each HV-pulse was  $\tau_{\text{HV-pulse}} = 80 \text{ }\mu\text{s}$ . Within this pulse duration, five retarded ignitions take place, so that an effective repetition rate of  $f_{\text{eff}} = 35 \text{ kHz}$  is resulting. In this mode of operation, the averaged plasma power is  $P_{\text{plasma}} = 1.19 \text{ W}$  and the pulse energy of each pulse amounts to  $E_{\text{HV-pulse}} = 0.17 \text{ mJ}$  as determined using the Lissajous-algorithm [26, 27]. Taking the plasma beam diameter into account, the plasma fluence is thus  $F_{\text{plasma}} = 0.54 \text{ J cm}^{-2}$  [10, 28]. Figure 2 shows a quantitative representation of the current and voltage waveforms of the plasma. Here,  $i_q$  is the current,  $u_d$  is the voltage across the dielectric,  $u_t$  is the total voltage and  $u_g$  is the voltage across the discharge gap. At the resulting operating parameters, the plasma gas temperature amounts to  $88 \text{ }^\circ\text{C}$  as determined in previous work [9].

As laser source, a Ti:sapphire-based regenerative amplifier system (Mantis seed laser from Coherent and Spitfire amplifier from Spectra Physics) at a central wavelength of  $\lambda_{\text{laser}} = 800 \text{ nm}$ , a laser pulse duration of  $\tau_{\text{laser}} = 60 \text{ fs}$ , and a repetition rate of  $f_{\text{laser}} = 10 \text{ kHz}$  was employed. The laser beam was focused by a lens with a focal length of  $f_{\text{lens}} = 500 \text{ mm}$  and guided coaxially to the plasma beam as shown in figure 1. The beam waist diameter (intensity  $1/e^2$ ) was  $2w_0 = 80 \text{ }\mu\text{m}$ , resulting in a Rayleigh length of  $z_R = 6.3 \text{ mm}$ .

For the ablation experiments the aluminium samples were moved perpendicularly to the laser focus, keeping the laser focus always on the surface with a constant distance. Two kinds of experiments were performed, (i) the combination of laser with assisting plasma and (ii) laser ablation in absence of plasma in order to identify the influence of the plasma on the ablation process and machining results. The sample material was aluminium AlMg3 (EN AW-5754 according to DIN EN 573-3) with a thickness of  $1 \text{ mm}$  and a lateral size of  $20 \times 20 \text{ mm}^2$ . The samples were placed on a motorised

xy-stage. By varying the stage's scan speed  $v$  and the laser power  $P_{\text{laser}}$ , respectively, different numbers of pulses and energies per unit length were applied to the sample surface. In a first step, single lines were engraved with laser pulse energies of  $E_{\text{laser}} = 100 \text{ }\mu\text{J}$  and a repetition rate of  $f_{\text{laser}} = 10 \text{ kHz}$ . The radiant exposure  $H$  of the material is then given by

$$H = \frac{N \cdot E_{\text{laser}}}{\pi \cdot r^2} \quad (1)$$

where  $N$  is the number of pulses per spot and  $r$  is the spot radius of the focussed laser on the surface of the aluminium sample. The number of pulses  $N$  is adjusted via the scan velocity  $v$  with

$$N = f_{\text{laser}} \cdot \frac{2 \cdot r}{v}. \quad (2)$$

The scan speeds were  $v = 0.1, 1, 2, 4, 6, 8,$  and  $10 \text{ mm s}^{-1}$ . Consequently, any spot on the laser treated surface was hit by 8000, 800, 400, 200, 133, 100, and 80 laser pulses, respectively.

Moreover, patterns of parallel lines with an overall dimension of approx.  $10 \times 10 \text{ mm}^2$  were engraved as presented in section 3.2. The scan speed was  $v = 0.57 \text{ mm s}^{-1}$  with a line spacing of  $70 \text{ }\mu\text{m}$ . For these patterns, two different laser parameter sets were applied: One sample was structured at a radiant expose of  $H = 943 \text{ J cm}^{-2}$  ( $N = 500$  pulses per spot,  $f_{\text{laser}} = 3.3 \text{ kHz}$ ). The other one was engraved at a radiant expose of  $H = 8952 \text{ J cm}^{-2}$  ( $N = 1600$  pulses per spot,  $f_{\text{laser}} = 10 \text{ kHz}$ ). It was further investigated whether the plasma has an impact on the laser ablation threshold. For this purpose, single lines were engraved on the sample surface at a fix scan speed of  $v = 5 \text{ mm s}^{-1}$  corresponding to 160 pulses per spot. The laser fluence was logarithmically decreased by varying the optical density linearly by the use of a neutral wedge in 30 steps from  $F_{\text{laser}} = 1.7 \text{ J cm}^{-2}$  to  $F_{\text{laser}} = 0.06 \text{ J cm}^{-2}$ .

The evaluation of the laser-engraved lines and structures was carried out by different techniques: First, a scanning electron microscope (SEM) (EVO MA10 from Zeiss) with an integrated energy-dispersive x-ray spectroscopy (EDX) device was used in order to analyse the laser-engraved structures visually and to determine the chemical composition of laser-induced debris, i.e. re-solidified material which is deposited on the sample surface. Second, the sizes and depths of laser-engraved structures were measured with the aid of a laser scanning microscope (LSM) (LSM 700 from Zeiss) where the measuring wavelength was  $405 \text{ nm}$  and the lateral resolution was  $250 \text{ nm}$ .

### 3. Results

#### 3.1. Plasma-assisted laser engraving of single lines

As determined by the LSM evaluation of single lines which were generated with 160 pulses per spot, the additionally applied APP does not affect a decrease in the laser ablation threshold of aluminium. The ablation threshold was rather slightly increased from  $F_{\text{laser}} = 0.06 \text{ J cm}^{-2}$  (pure laser engraving) to  $F_{\text{laser}} = 0.17 \text{ J cm}^{-2}$  (APP-assisted

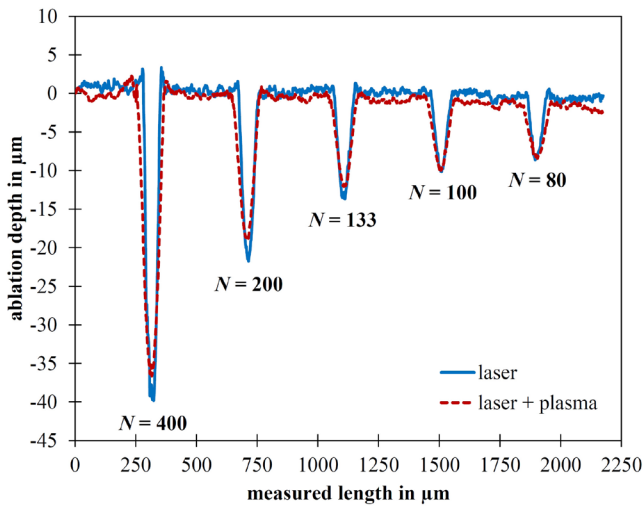


**Figure 3.** Comparison of cross sections of laser-engraved lines realised at a fluence of  $F_{\text{laser}} = 2.0 \text{ J cm}^{-2}$  for different numbers of pulses per spot  $N$  with (dashed line) and without (solid line) assisting plasma.

laser engraving). It was further observed that in the case of engraving single lines at fluences of  $F_{\text{laser}} = 2.0 \text{ J cm}^{-2}$ , i.e. well above the ablation threshold the plasma does not significantly influence the amount of ablated volume for a different number of pulses per spot. As shown by the comparison of the cross sections of laser-engraved lines as measured by LSM in figure 3 and the particular values for the ablation depth and line width, respectively in figure 4, the ablation depth was marginally decreased whereas the line width was increased.

For more than 400 pulses per spot (corresponding to  $H = 795 \text{ J cm}^{-2}$ ) the laser-engraved lines could not be evaluated quantitatively due to the high aspect ratio and the resulting distortion of the LSM measurement signal by multiple reflexions within the structures.

Even though no significant difference in terms of the ablated volume was observed, the plasma has a notable influence on the nature of resulting structures as shown in figure 5. In case of pure ablation, several spikes were formed at the bottom on the lines which is a typical behaviour in the case of femtosecond-laser ablation of aluminium [17, 20, 23, 29, 30]. However, such spikes were not observed when introducing the D-DBD plasma to the laser process. Here, much more debris was deposited on the line edges and on the sample surface.

### 3.2. Plasma-assisted laser engraving of patterns

Generally, in contrast to engraving single lines, the overall ablation depth is notably increased when writing areas as shown in figure 6. In case of pure laser treatment, nearly no material was ablated for both 500 and 1600 pulses/spot. The aluminium surface was rather roughed up within a depth range of some microns. When introducing the plasma to the ablation process, the overall ablation depth was increased. In relation to the untreated sample surface, the ablation depth amounts to a mean value of approx.  $20 \mu\text{m}$  at  $F_{\text{laser}} = 2.0 \text{ J cm}^{-2}$  applied with 500 pulses/spot and  $250 \mu\text{m}$  at  $F_{\text{laser}} = 6.0 \text{ J cm}^{-2}$  with 1600 pulses/spot, respectively.

In addition to an increase in overall ablation depth, the plasma has strongly influenced the structure at the bottom of the ablated patterns as shown in figure 7. This behaviour was also qualitatively observed for single laser-engraved lines, compare section 3.1 and figure 5. On the sample structured with 500 pulses/spot, the peak-to-valley height (PV) of these structures was approx.  $10 \mu\text{m}$  for both pure laser ablation and plasma-assisted ablation. Randomly-distributed surface roughening with structure sizes in the range of some microns to some tens of microns was also resulting from pure laser ablation at samples structured at  $F_{\text{laser}} = 6.0 \text{ J cm}^{-2}$  with 1600 pulses/spot. However, conoidal peaks with lateral sizes of several tens of microns and a peak-to-valley height of up to approx.  $100 \mu\text{m}$  were observed in the case of plasma-assisted structuring on these samples. These peaks feature steep flanges with a relatively high surface roughness.

During plasma-assisted ablation, a film of powdery, whitish debris particles was formed on the sample surface. This film could easily be wiped away and was thus not adhered to the surface. As ascertained by EDX measurements, the observed film of particles on the sample surface which occurred only in the case of plasma-assisted ablation contains a considerable amount of carbon and oxygen, the latter indicating a plasma-induced formation of oxidised aluminium. For the pure aluminium surface, only aluminium and magnesium and a small amount of oxygen was detected by EDX as listed in table 1. These elements are the main compounds of the investigated material, AlMg3.

## 4. Discussion

The observed increase in ablation threshold and the differences in ablation depths and widths of laser-engraved lines can be explained by a slight defocusing of the laser beam by the plasma. As a result of such defocusing, the fluence on the sample surface is reduced. As reported in previous work, a focused laser beam is subject to a focus shift of approx.  $2.8 \text{ mm}$  when passing a D-DBD plasma beam which is driven at a nominal pulse repetition rate of  $7 \text{ kHz}$ . This behaviour is due to an increase in gas temperature within this plasma beam of approx.  $13 \text{ K}$  with respect to the ambient air temperature [31]. Since an increase in air temperature comes along with a decrease in its refractive index [32], the cylindrical plasma beam acts as defocusing thermal gradient index lens. However, the focal shift is much lower than the Rayleigh length of  $z_R = 6.3 \text{ mm}$ .

The plasma-induced increase in overall ablation depth which was observed for laser-engraved patterns is most likely due to an improved removal of aluminium particles due to the electric field of the D-DBD plasma. Okano *et al* have shown that during femtosecond laser ablation of aluminium, the expansion velocity of vaporised aluminium and condensed aluminium particles amounts to  $10^4 \text{ m s}^{-1}$  and  $10^3 \text{ m s}^{-1}$ , respectively. Without assisting plasma, ablated aluminium particles slow down rapidly (within some tens of nanoseconds [33]) and remain in the immediate vicinity (some hundreds of microns) of the cutting point close to the ablated surface

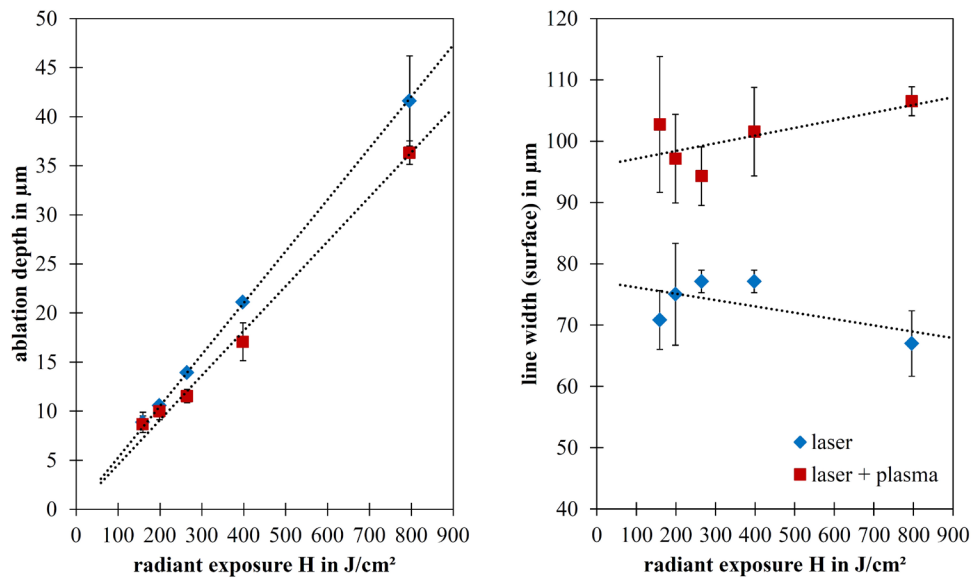


**Figure 4.** Ablation depth (left) and line width on the sample surface (right) of laser-engraved lines with and without assisting plasma versus radiant exposure. (The dotted lines represent the particular trends and were added for better visualisation.)

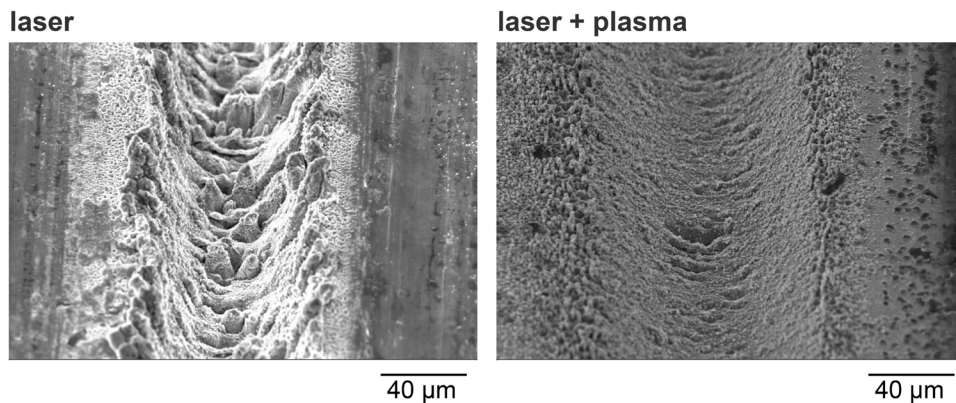


**Figure 5.** Comparison of laser-engraved lines on aluminium without (left) and with assisting plasma (right), engraved at a constant energy per unit length of  $500 \text{ J mm}^{-1}$ .

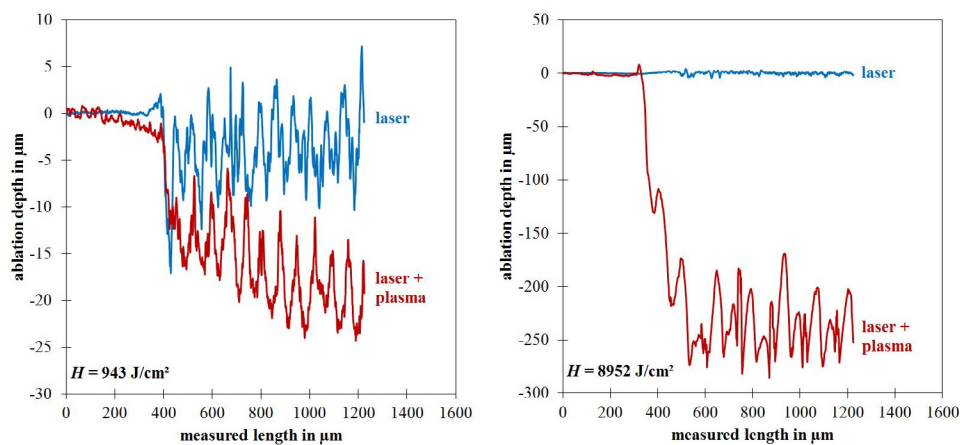


**Figure 6.** Cross sections of patterns on aluminium realised by laser engraving at a radiant exposure of  $H = 943 \text{ J cm}^{-2}$  (left), and  $H = 8952 \text{ J cm}^{-2}$  (right), respectively, with and without assisting plasma; the structure edge is found at a measured length of approx. 350 microns. Please note the different scaling of the y-axes.

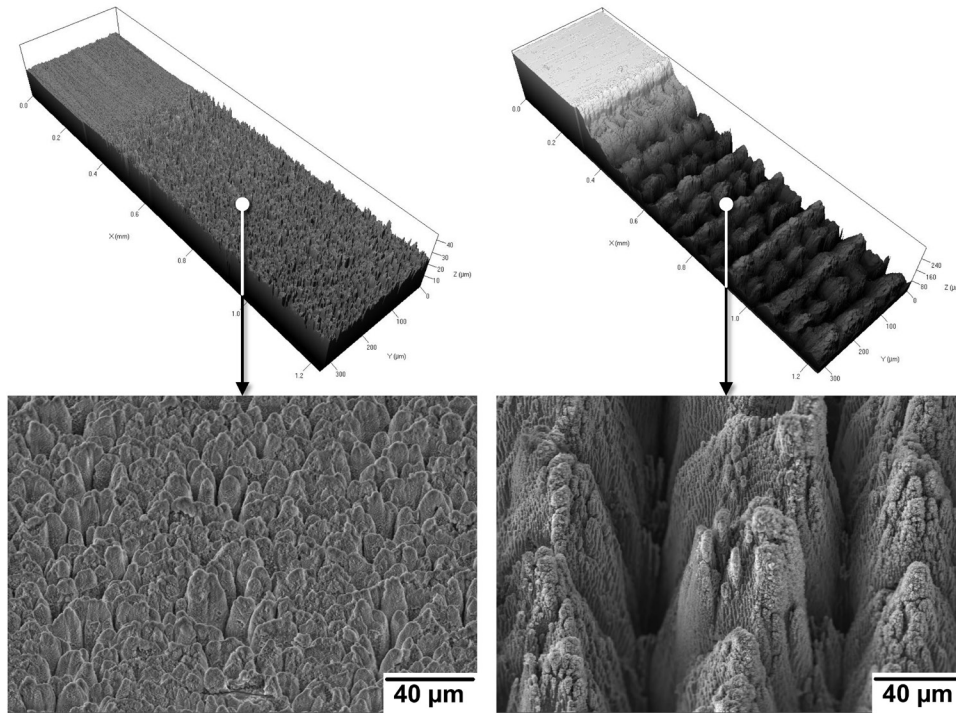


**Figure 7.** Comparison of LSM- (top) and SEM-pictures (bottom) of micro-structures on the bottom of laser-engraved patterns without (left) and with assisting plasma (right); the laser parameters were  $F_{\text{laser}} = 6.0 \text{ J cm}^{-2}$  and 1600 pulses/spot.

**Table 1.** EDX analysis of aluminium sample surface and deposited debris.

Element	Content in at. %	
	Aluminium sample	Deposited debris
Aluminium (Al)	92.7	68.8
Oxygen (O)	3.9	18.5
Magnesium (Mg)	3.4	2.9
Carbon (C)	—	9.7

where a re-deposition takes place after the actual ablation process between two laser pulses.

In contrast, the particles are removed by the assisting plasma and are even found on the sample surface at a distance of several centimetres from the cutting point in the form of a film of powdery debris particles. This plasma-induced removal effect can be explained as follows: Since the sample is placed within the discharge gap, a Debye sheath layer is formed on the sample surface and at the bottom of the ablated area, respectively. The sample's surface charge is thus negative due to the higher mobility of electrons in comparison to heavy particles such as ions. Further, the electric field of the sheath causes the formation of a dipole field on the particles [34, 35] and a negative charging. The surface charge of the sample leads to a repulsion of negatively-charged aluminium particles, consequently removing these particles from the cutting point. This effect is supported by the fact that the effective repetition rate of the plasma (35 kHz) is 3.5-times higher than the repetition rate of the laser (10 kHz), resulting in several periodical ignitions of the D-DBD plasma in between two incident laser pulses.

In addition to the formation of a dipole field, oxidation of the particles can contribute to repulsion processes. Such oxidation and the formation of a natural oxide layer on the particle surface are indicated by the presence of oxygen within the debris film as ascertained via EDX. For the formed particle layer, a significantly larger amount of oxygen was found with respect to the aluminium surface (approx. 4.7 times higher). Further, a certain percentage of carbon was detected. This can be explained by a mixing of aluminium particles with hydrocarbons from the ambient air. The EDX analysis clearly indicates basic differences in the particular ablation processes. Apparently, the plasma transfers energy into the removed aluminium particles and induces chemical reactions (oxidation and carbonisation) of these particles. As a result of a passivation of the particles by oxidation, the influence of electrostatic effects which arise from the plasma ignition is higher for oxidised particles. This fact could contribute to the removal of particles by the alternating electric field within the discharge gap. Moreover, a reduction in density and a change in surface tension of the particles could support this mechanism.

The removal of particles from the cutting point directly impacts the ablation efficiency. In case of dense particle clouds, the laser beam is subject to scattering and absorption at such particles. These loss mechanisms give rise to a shadowing of the incident laser beam and lower its power and fluence on the sample surface, respectively. The observed dependency of the overall ablation depth on the laser power could be explained by the fact that for higher laser powers, more particles are generated. As reported by Zhang *et al*, such increased material injection is found in the intense femtosecond laser ablation (i.e.  $F > 40 \text{ J cm}^{-2}$ ) regime during ablation of aluminium [36]. In the present work, the

maximum laser fluence was  $6 \text{ J cm}^{-2}$ . However, 1500 pulses per spot were applied at this fluence, resulting in a laser dose of  $9 \text{ kJ cm}^{-2}$  (i.e. the product of the number of laser pulses and the fluence). Ablation was thus performed within the above-mentioned intense ablation regime. As a result, the laser beam is significantly shadowed in case of pure laser ablation. In contrast, the removal of particles by the plasma improves the total energetic efficiency of the ablation process. This behaviour was also qualitatively observed in previous work where plasma-assisted UV-nanosecond laser ablation of aluminium was investigated [12]. It was moreover recently shown by particle size distribution measurements that the use of assisting D-DBD-plasma during picosecond laser ablation of titanium leads to a significant decrease in particle size [37], contributing to a decrease in attenuation of the incident laser beam by the formed debris cloud due to scattering, absorption and reflection. The impact of such attenuation is a well-known effect in laser materials processing and may lead to a severe reduction in laser ablation efficiency. For instance, a reduction in ablation depth by a factor of up to 14 was observed in the case of ablation of fused silica in previous work [38]. Here, the above-mentioned factor follows from the difference in ablation depth for front side (low ablation depth) and rear-side (high ablation depth) ablation.

Another effect which potentially contributes to an increase in ablation rate may be an additional energy transfer by the de-excitation of argon metastables. The use of argon as plasma process gas in D-DBD configurations results in the formation of excited argon atoms and metastable argon species within the plasma volume. The latter species features an energy of approx. 11.5 eV which is lost by radial diffusion and de-excitation at walls [39]. In a D-DBD, the only wall involved is given by the surface of the work piece. The resulting energy transfer into its surface could considerably contribute to simultaneously combined APP-laser processes [10–12].

In addition to an increase in ablation depth, the surface geometry of engraved lines and patterns is strongly influenced by the plasma. For large-scale patterns, the surface geometry corresponds quite well to the expected structure which should result from the scanning parameters and procedure (i.e. a beam waist diameter of  $2w_0 = 80 \text{ }\mu\text{m}$  and a line spacing of  $70 \text{ }\mu\text{m}$ ) as shown in figure 7. In contrast, a randomly-distributed surface structure was resulting from pure laser ablation. Anyhow, the formation of spikes with steep flanges during plasma-assisted laser engraving of patterns could further contribute to the observed increase in overall ablation depth by ‘trapping’ incident laser irradiation. Such flanges give rise to multiple reflexions and can thus provoke additional coupling of laser energy into the surface. The high surface roughness of the flanges further results in an increase in diffusively reflected laser irradiation [40] and an additional coupling into the surface, respectively.

## 5. Conclusions

The experimental results presented in this contribution show that introducing D-DBD argon plasma at atmospheric pressure to femtosecond laser ablation of aluminium simultaneously



does not reduce the ablation threshold. It was further observed that the ablation rate is not increased when engraving single lines. However, the overall ablation rate is notably increased when inscribing patterns consisting of parallel overlapping lines. This fact indicates that a plasma-induced increase in ablation rate is directly related to an accumulation of ablated particles. Here, the removal of such particles from the cutting point by the plasma is supposed to be the main mechanism for the observed increase in ablation depth by a factor of up to 250 (at  $P_{\text{laser}} = 3 \text{ W}$ ). Several possible underlying active principles are suggested: a removal of charged particles by the negatively-charged sheath on the sample surface and the alternating electric field within the discharge gap (supported by an oxidation of particles as ascertained by EDX) as well as an additional energy input into the surface by (i) the de-excitation of metastable plasma species and (ii) multiple reflexions that result from both the formation of spikes with steep flanges and the surface roughness of those spikes. In any case, the plasma has a notable influence on the resulting surface geometry.

Such plasma-induced increase in effective surface area (compare figure 7) has a number of possible practical applications as for example the realisation of passive cooling elements, catalytic electrode materials or substrates for surface enhanced Raman spectroscopy (SERS). The increase in overall ablation depth has a clear potential for enhancing the efficiency and machining speed of femtosecond laser-based material processing and structuring processes. The admixture of additional working gases such as oxygen to the carrier gas argon used in the present work may even result in a further improvement of the results and will be investigated in future work.

## Acknowledgments

The financial support by the Ministry for Science and Culture of Lower Saxony in the frame of the pilot study ‘LUPS’ and the European Regional Development Fund in the frame of the project ‘SNIFF’ is gratefully acknowledged.

## ORCID iDs

Christoph Gerhard  <https://orcid.org/0000-0002-6837-2498>  
Wolfgang Viöl  <https://orcid.org/0000-0003-3425-9937>

## References

- [1] Brückner S, Hoffmeister J, Ihlemann J, Gerhard C, Wieneke S and Viöl W 2012 *J. Laser Micro/Nanoeng.* **7** 73–6
- [2] Gerhard C, Tasche D, Brückner S, Wieneke S and Viöl W 2012 *Opt. Lett.* **37** 566–8
- [3] Gerhard C, Weihs T, Tasche D, Brückner S, Wieneke S and Viöl W 2013 *Plasma Chem. Plasma Process.* **33** 895–905
- [4] Tasche D, Gerhard C, Ihlemann J, Wieneke S and Viöl W 2014 *J. Eur. Opt. Soc. Rapid Publ.* **9** 14026
- [5] Mainusch N, Pflugfelder C, Ihlemann J and Viöl W 2007 *Plasma Process. Polym.* **4** S33–8
- [6] Schmiedel C, Schmiedel A and Viöl W 2009 *Proc. 19th Int. Symp. on Plasma Chemistry (IPCS19)* pp 239–43



- [7] Pflugfelder C, Mainusch N, Ihlemann J and Viöl W 2008 *Proc. 7th Int. Conf. on Lasers in the Conservation of Artworks (LACONA VII)* pp 55–8
- [8] Le Meur V, Loewenthal L, Gerhard C and Viöl W 2015 *Laser Ablation: Fundamentals, Methods and Applications* (Hauppauge: Nova Science Publishers) pp 165–77
- [9] Gredner A, Gerhard C, Wieneke S, Schmidt K and Viöl W 2013 *J. Mater. Sci. Eng. B* **3** 346–51
- [10] Gerhard C, Roux S, Brückner S, Wieneke S and Viöl W 2012 *Appl. Opt.* **51** 3847–52
- [11] Gerhard C, Roux S, Peters F, Brückner S, Wieneke S and Viöl W 2013 *J. Ceram. Sci. Technol.* **4** 19–24
- [12] Gerhard C, Roux S, Brückner S, Wieneke S and Viöl W 2012 *Appl. Phys. A* **108** 107–12
- [13] Sugioka K and Cheng Y 2014 *Light Sci. Appl.* **3** e149
- [14] Gamaly E G 2011 *Femtosecond Laser-Matter Interaction: Theory, Experiments And Applications* (Boca Raton, FL: CRC Press)
- [15] Gamely E G, Madson N R, Duering M, Rode A V, Kolev V Z and Luther-Davies B 2005 *Phys. Rev. B* **71** 174405
- [16] He S, Nivas J J, Vecchione A, Hu M and Amoruso S 2016 *Opt. Express* **24** 3238–47
- [17] Vorobyev A Y and Guo C 2015 *J. Appl. Phys.* **117** 33103
- [18] Gimpel T, Guenther K-M, Kontermann S and Schade W 2014 *Appl. Phys. Lett.* **105** 053504
- [19] Crouch C H, Carey J E, Shen M, Mazur E and Génin F Y 2004 *Appl. Phys. A* **79** 1635–41
- [20] Korte F, Nolte S, Chichkov B N, Bauer T, Kamlage G, Wagner T, Fallnich C and Welling H 1999 *Appl. Phys. A* **69** S7–11
- [21] Wu B, Zhou M, Li J, Ye X, Li G and Cai L 2009 *Appl. Surf. Sci.* **256** 61–6
- [22] Baldacchini T, Carey J E, Zhou M and Mazur E 2006 *Langmuir* **22** 4917–9
- [23] Yang Y, Yang J, Liang C and Wang H 2008 *Opt. Express* **16** 11259–65
- [24] Paivasaari K, Kaakkunen J J J, Kuittinen M and Jaaskelainen T 2007 *Opt. Express* **15** 13838–43
- [25] Brückner S, Rösner S, Gerhard C, Wieneke S and Viöl W 2011 *Mater. Test.* **53** 639–42
- [26] Manley T C 1943 *ECS Trans.* **84** 83–96
- [27] Helmke A, Hoffmeister D, Mertens N, Emmert S, Schuette J and Viöl W 2009 *New J. Phys.* **11** 115025
- [28] Gerhard C, Weihs T, Luca A, Wieneke S and Viöl W 2013 *J. Eur. Opt. Soc. Rapid Publ.* **8** 13081
- [29] Lu Y F, Yu J J and Choi W K 1997 *Appl. Phys. Lett.* **71** 3439–40
- [30] Nayak B K and Gupta M C 2010 *Opt. Lasers Eng.* **48** 940–9
- [31] Hoffmeister J, Brückner S, Gerhard C, Wieneke S and Viöl W 2014 *Plasma Sources Sci. Technol.* **23** 064008
- [32] Edlén B 1966 *Metrologica* **2** 71–80
- [33] Okano Y, Oguri K, Nishikawa T and Nakano H 2006 *Appl. Phys. Lett.* **89** 221502
- [34] Lee H C, Chen D Y and Rosenstein B 1997 *Phys. Rev. E* **56** 4596–607
- [35] Lapenta G 1999 *Phys. Plasmas* **6** 1442–7
- [36] Zhang N, Zhu X, Yang J, Wang X and Wang M 2007 *Phys. Rev. Lett.* **99** 167602
- [37] Grottke S, Viöl W and Gerhard C 2017 *Appl. Opt.* **56** 3365–71
- [38] Hoffmeister J, Gerhard C, Brückner S, Ihlemann J, Wieneke S and Viöl W 2012 *Phys. Procedia* **39** 613–20
- [39] Bogaerts A and Gijbels R 1997 *Spectrochim. Acta B* **52** 553–65
- [40] Bennett H E and Porteus J O 1961 *J. Opt. Soc. Am.* **51** 123–9